



Microstructural origins for quench cracking of a boron steel: Boron distribution

Jie Bai^a, Shenbao Jin^{a,*}, Chuan Liang^b, Xiang Li^b, Zesheng You^a, Yonghao Zhao^a, Lihua Liu^b, Gang Sha^{a,*}

^a Herbert Gleiter Institute of Nanoscience, School of Materials Science and Engineering, Nanjing University of Science and Technology, Nanjing 210094, China

^b Nanjing Iron and Steel Co., Ltd, Nanjing 210000, China

ARTICLE INFO

Keywords:

Boron steel
B distribution
Precipitates
Quench cracking
Atom probe tomography

ABSTRACT

Boron is an important trace element and intentionally added for hardenability of low-alloy steels. The forms of B presence in microstructure are believed to be crucial for success or failure of boron steel production. This research addresses atomistic distribution of boron responsible for quench cracking of a boron steel. Boron steel sheets (6 mm thick) with/without quench cracking are carefully characterized with transmission electron microscopy and atom probe tomography to reveal B distribution and to understand quench cracking mechanisms. The quench cracking is brittle intergranular fracture along prior austenite grain boundaries (PAGBs). The PAGBs are decorated with boron-containing Fe₃(C, B) precipitates in the cracked steel, but segregated with boron in the uncracked steel. Without the segregation of B at PAGBs, the formation of ferrite and massive acicular-shaped Fe₃C during quenching makes cracks easy to initiate and propagate in the steel with deteriorated mechanical properties. Processing parameters important for engineering the distribution of boron are discussed.

1. Introduction

Boron steels are an important class of high-strength low-alloy steels with addition of trace B for enhanced hardenability and full martensitic structure to save in using expensive alloying elements [1]. Adding 10–30 wt ppm boron could produce a hardening effect comparable to that obtained by adding 0.6 wt% Mn, 0.7 wt% Cr, 0.5 wt% Mo or 1.5 wt% Ni [2]. The beneficial effect of boron on hardenability is believed resulting from the segregation of boron atoms at austenite grain boundaries to lower the grain boundary energy and retard the nucleation of ferrite and bainite [3–11]. However, boron can easily react with carbides and nitrogen to form metal borocarbides and boron nitrides in steels during high-temperature processing [12]. The formation of these precipitates consumes boron atoms segregating at austenite grain boundaries, and loses the beneficial effect of boron addition on hardenability. Moreover, the boron-containing precipitates such as M₂₃(B,C)₆ or coarse BN formed along PAGBs promote ferrite nucleation [13–17], and reduce the percentage of martensite in microstructure and mechanical properties of the steels. Some research suggests that BN and iron borocarbide particles can also increase the brittleness of the grain boundaries and induce intergranular fracture during continuous casting and subsequent heat

treatments [18–22]. Therefore, engineering boron distribution is of significance for industrial production of the boron steels.

Quench cracking is an important failure mode in steel production. It may occur under high internal stress incurred by the phase transformation from austenite to martensite. Boron addition shifts the ferrite zone in the continuous cooling transformation (CCT) diagram to the right, but does not decrease the martensite start temperature (M_s point) [1,23]. Given that the tendency of quench cracking increases with the decrease in the M_s point, boron steels are generally believed to be less susceptible to quench cracking [24]. However, quench cracking of boron steel sheets does happen unexpectedly on their production line. To date, precise mechanisms of such quench cracking remain to be uncovered. Key microstructures responsible for the quench cracking remain to be explored. The lack of deep knowledge about the quench cracking becomes a major obstacle for finding effective measures to solve the cracking problem.

This investigation is to address quenching cracking of a boron steel containing 15 wt ppm boron. To reveal the key microstructural factors responsible for the quench cracking, multi-scale characterizations including SEM, TEM and APT have been carefully performed on two steel sheets with/without quench cracking. By revealing microstructural

* Corresponding authors.

E-mail addresses: jinshenbao@njust.edu.cn (S. Jin), gang.sha@njust.edu.cn (G. Sha).

<https://doi.org/10.1016/j.matchar.2022.112022>

Received 7 February 2022; Received in revised form 27 May 2022; Accepted 28 May 2022

Available online 2 June 2022

1044-5803/© 2022 Published by Elsevier Inc.

difference between the two sheets and local boron distribution information, this investigation will establish the correlation between microstructural characteristics and quench-cracking behavior of the boron steel.

2. Experimental procedures

Boron steel sheets with a thickness of 6 mm were used in this work, with chemical composition listed in Table 1. The sheets were austenitized at 880 °C for 30 min and then quenched by water jet to room temperature. During the quenching, some sheets fractured seriously and broke into several pieces, as shown in Fig. 1. The mechanical properties and microstructure of the cracked sheet (hereafter referred to as the “cracked sample”) and an uncracked sheet after quenching (referred to as the “uncracked sample”) were analyzed.

The mechanical properties at different positions across the thickness of the steel sheet were characterized via tensile test and impact test. Fig. 2a shows the sampling plan to make tensile and impact specimens along the rolling direction from different depths of the boron steel sheet (i.e. evenly divided five parts in thickness of the steel sheets). The dimensions of the standard tensile specimens and impact test specimens are shown in Fig. 2b and c, respectively. The tensile test was performed at room temperature under a constant speed of 0.9 mm/min using Walter + bai LFM 20kN tensile test machine. The impact test was carried out at room temperature with an impact energy 50 J and a pendulum angle 150° on Walter + bai PH 25–50 J pendulum impact test machine.

Optical microscopy (OM), scanning electron microscopy (SEM), transmission electron microscopy (TEM) and atom probe tomography (APT) were utilized for microstructural characterization. The metallographic specimens of the cracked and uncracked samples were subjected to mechanical polishing, and then etched in ET-08, a substitute for saturation picric acid to reveal prior austenite grains, or etched by 4% Nital solution to reveal martensite structure for optical microscopy observations. Metallography examinations were performed using a Leica DMI 5000 M. SEM examinations were performed using a ZEISS Auriga crossbeam system. TEM analysis was conducted using a FEI Talos F200S G2 equipped with energy dispersive spectrometer (EDS) under an acceleration voltage of 200 kV. TEM foil specimens of 3 mm in diameter were prepared using a twin-jet electro-polisher (Struers TenuPol-5).

APT tip specimens containing prior-austenite grain boundaries (PAGBs) were prepared by focused ion beam (FIB) milling using a ZEISS Auriga Crossbeam system. APT experiments were conducted with a local electrode atom probe LEAP 4000× Si, at a UV laser energy of 40 pJ, a specimen temperature of 40 K and a vacuum 4×10^{-11} Torr. Data reconstruction and analysis were conducted on the software package IVAS version 3.8.2. The 3D reconstruction of APT dataset was based on tip shape information (apex diameter, sample taper, etc.) obtained by SEM imaging.

3. Results

3.1. Fractography of quench cracking

Fig. 3a shows a picture of the quench-cracked steel sheet with fracture surface regions for detailed microstructural examinations. The fracture region near a side edge of the steel sheet consists of three segments approximately perpendicular to the side surface of the cracked steel sheet. Two vertical segments (marked with surface 1 and 2) are perpendicular to the sheet surface and a transverse segment (marked



Fig. 1. Quench-cracked boron steel sheet with a thickness of 6 mm.

with surface 3) is parallel to the sheet surface. The main fracture region away from the edge of the steel sheet only has a vertical straight segment along the thickness direction. Since the formation of the transverse segment required additional energy, the fracture near the edge region should consume more energy than single straight segment. The topography of the fracture surfaces under SEM, as shown in Fig. 3b–d, demonstrates that the fracture is brittle in nature with fracture surfaces in a “rock candy” appearance, probably correlated with intergranular fracture. Some secondary microcracks, as pointed with white arrows in Fig. 3b and c, are evidenced underneath the main fracture surface and again faceted in nature.

A large secondary crack, as shown in Fig. 3e, penetrated deeply into the steel substrate below the main fracture surface. The propagation of the secondary crack is associated with micro-cracks clearly along PAGBs, as observed by using SEM in Fig. 3f. It is thus concluded that the PAGBs are directly responsible for the initiation and propagation of quench cracks in the cracked sample. The occurrence of brittle intergranular fracture must be due to that the PAGBs between the austenite grains were seriously weakened during quenching.

3.2. Mechanical properties of the steel with/without quench cracking

Fig. 4a shows the true stress-strain curves for tensile specimens taken from different depths along the thickness of the uncracked and cracked samples. The tensile strengths and elongation rates of the uncracked steel were significantly higher than those of the cracked sample, no matter near the surface or close to the center of the steel sheets. Both the uncracked and cracked steels showed no considerable change in tensile properties along the thickness of each steel, indicating a uniform distribution of tensile properties across the thickness. The uncracked and the cracked samples had average yield strengths of 1910.6 ± 27.75 MPa and 1406.8 ± 75.12 MPa, respectively, average ultimate tensile strengths of 2100.8 ± 36.19 MPa and 1465.1 ± 76.12 MPa, respectively, and average elongation rates of $4.0 \pm 0.2\%$ and $2.5 \pm 0.3\%$, respectively. Interestingly, the quench-cracked steel exhibited strain hardening lower than that of the uncracked steel. This means that localized deformation should be harder to propagate in the quench-cracked steel, and hence the cracked steel exhibits a low elongation rate.

Fig. 4b displays the impact energies of specimens from different

Table 1

Chemical composition of a boron steel (wt% and at.%).

| | C | Ni | Mn | Mo | Si | Cr | P | Ti | B | Fe |
|------|------|------|------|------|------|------|-------|-------|--------|------|
| wt% | 0.33 | 0.83 | 0.80 | 0.45 | 0.31 | 0.28 | 0.006 | 0.015 | 0.0015 | 97.0 |
| at.% | 1.51 | 0.78 | 0.80 | 0.26 | 0.61 | 0.30 | 0.010 | 0.020 | 0.010 | 95.7 |

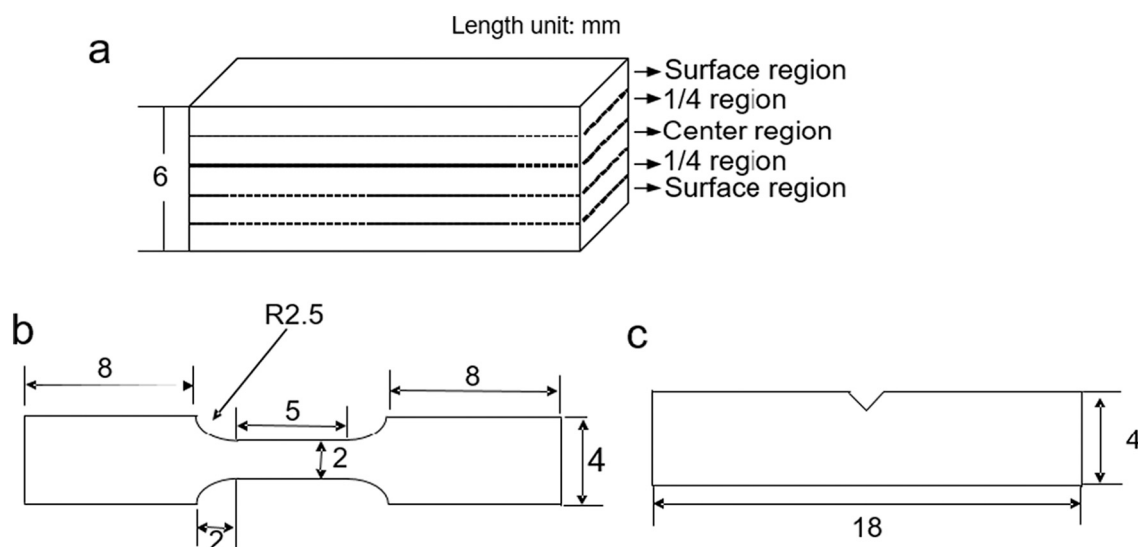


Fig. 2. Sampling scheme along thickness direction of uncracked and cracked samples for tensile and impact tests (a), and dimensions of tensile specimens (b) and impact specimens (c).

positions along thickness of the uncracked and cracked samples. The impact energies of specimens from different positions of the uncracked sheet (blue data points) do not change much, approximately 1.5 J. In contrast, the center of the cracked steel exhibited a poor impact toughness of ~ 1.0 J, much lower than ~ 1.5 J, the impact energy (in black) of the surface region of the cracked steel (Fig. 4b). To find out microstructural origins responsible for the poor tensile and impact properties of the quench-cracked steel, the microstructures of the uncracked steel and the cracked steel were carefully investigated.

3.3. Microstructure and phase constituents of the steel with/without quench cracking

Fig. 5a–c shows the microstructure of near surface and center regions in the uncracked and cracked samples with the prior austenite grains clearly resolved. The austenite grains of the three regions are all equiaxed but different in sizes. The cracked sample has austenite grains larger than that of uncracked sample, especially in the center region. The average sizes of prior austenite grains near the surface region of the uncracked sample, as well as near surface and center regions of the cracked sample were measured to be $6.4 \pm 0.7 \mu\text{m}$, $12.6 \pm 1.6 \mu\text{m}$ and $16.5 \pm 1.8 \mu\text{m}$, respectively, with the linear intercept method.

Fig. 5d–f shows microstructures of samples from the cracked or uncracked steel etched with a 4% Nital solution. The microstructure of the uncracked steel consists of typical lath martensite, as seen in Fig. 5d. The surface region in the cracked sample has a microstructure containing both lath martensite and a few block grains, referred as ferrite, in Fig. 5e. The center region of the cracked sample is a mixture of martensite and ferrite, as seen in Fig. 5f. The lath martensite and block ferrite are seen more clearly in the SEM images (Fig. 5g–i). The ferrite phase mainly distributed on the PAGBs. It is known that the ferrite in quenched microstructure can be caused by two routes: one is ferrite undissolved after austenitization treatment, and the other is ferrite precipitated before martensite transformation during quenching. Given that the undissolved ferrite mainly distribute in the interiors of the austenite grains, rather than on PAGBs [25], it is concluded that the ferrite in the cracked sample is freshly formed by precipitation during quenching. A full transformation to martensite would be secured if the steel with a good hardenability reached its critical cooling rate during quenching. The formation of the ferrite in the cracked sample indicated that either the cooling rate was too slow or the hardenability of the steel deteriorated.

3.4. Precipitation on PAGBs of the steel with/without quench cracking

TEM examinations of PAGBs in the uncracked and cracked samples, as shown in Fig. 6a and b, confirmed that no precipitate was found in the uncracked sample. In contrast, nano-sized precipitates with different morphologies exist in both the surface and center regions in the cracked sample (Fig. 6c–f). High number density of acicular-shaped precipitates formed on the PAGBs, martensite lath boundaries (MLB) and martensite matrix, while some spherical-shaped precipitates mainly observed on the PAGBs, as seen in Fig. 7a. The chemistry of the precipitates was measured with EDS point analysis in TEM, as seen in Fig. 7b and c. The carbon content of an acicular-shaped precipitate (P1) is close to 25 at.%, with an Fe:C ratio close to 3:1, similar to that of Fe_3C , as seen in Fig. 7d. In contrast, the spherical-shaped precipitate P2 on the PAGBs is enriched with boron, with 73.2 at.% Fe and 25.4 at.% (C + B) in P2 by EDS point analysis. P2 precipitate likely is $\text{Fe}_3(\text{C}, \text{B})$. It is worth noting that particles (P1 and P2) carefully selected for composition measurement were a large platelet rod with sizes of ~ 100 – 200 nm in length and 40 – 50 nm in thickness, to minimize the effect of the TEM foil thickness (< 100 nm), in EDS analysis with a prob. size of ~ 20 nm. Therefore, the composition of precipitates obtained by EDS analysis should be less affected by the surrounding matrix. The foil specimens have been plasma cleaned before TEM investigation to eliminate the possible carbonaceous contamination on surfaces. In addition, the martensite matrix composition has been measured using EDS. It is found that the carbon content in matrix measured by EDS is 0.66 – 1.30 at.%, comparable to that obtained by APT analysis (0.29 – 0.93 at.%), indicating that the carbon content gained using EDS is quite accurate. Therefore, the composition of precipitates obtained by EDS analysis on TEM foils should be reliable.

3.5. Elemental distribution at PAGBs

Elemental distribution at PAGBs in the uncracked and cracked samples was characterized using APT. Fig. 8a shows atom maps in a reconstructed volume of an APT dataset from the uncracked sample with a PAGB enriching with B, C, Mo and P, and a martensite lath boundary enriching with carbon and Mo. Fig. 8b and c shows the APT reconstructions with PAGBs in near surface and center regions of the cracked steel. The PAGB in near surface region of the cracked steel was observed with clear segregation of boron, carbon, Mo and P (see Fig. 8b), but the PAGB in the center region did exhibit no segregation with boron (see Fig. 8c). Actually, no boron was detected in the reconstructed

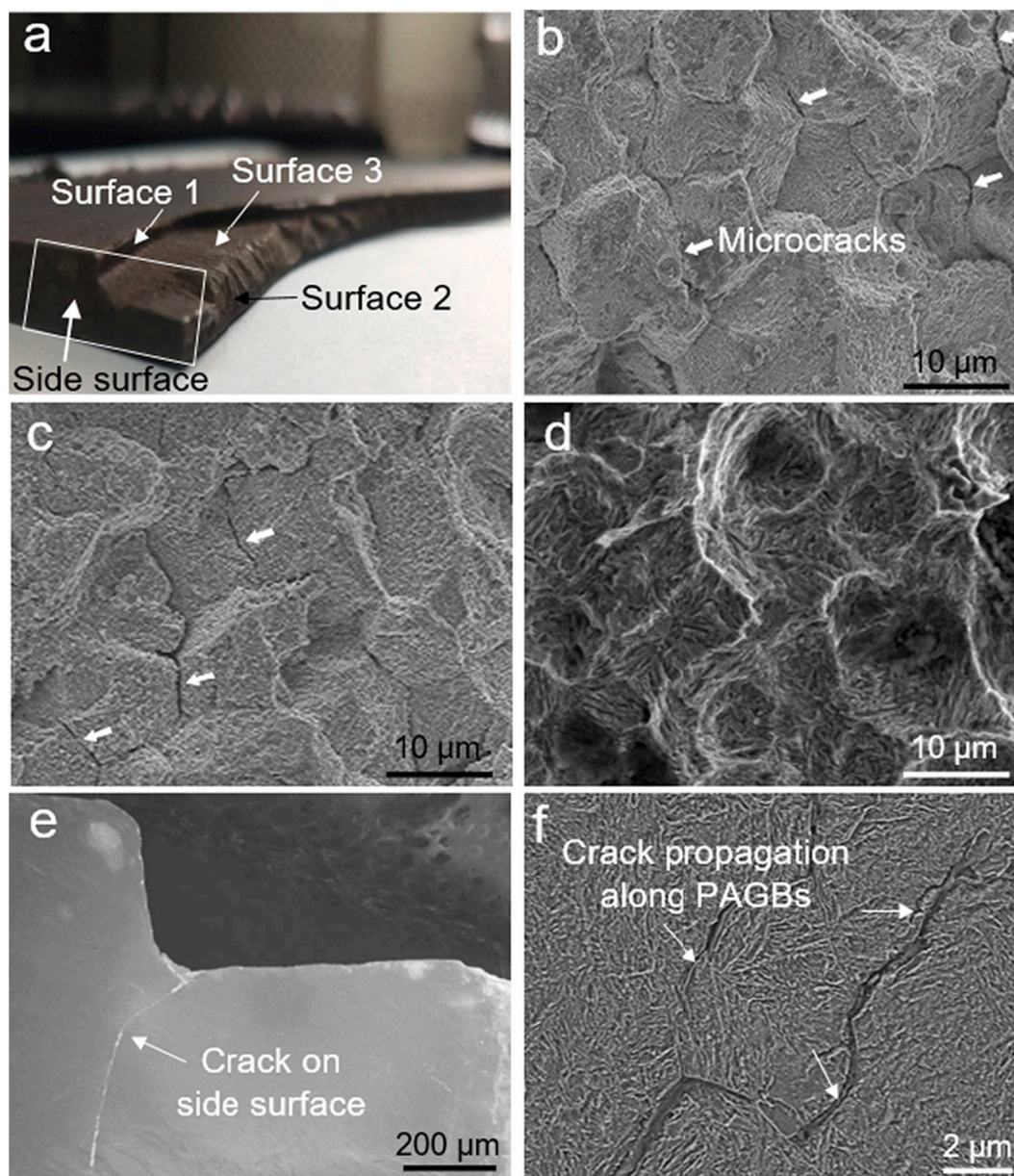


Fig. 3. A picture of the cracked steel sheet marked with three fracture surfaces for detailed SEM observations (a), SEM images of the fracture surfaces 1–3 (b)–(d), the side surface with micro-cracks (e), and propagation of the micro-cracks into the steel substrate (f).

volume in Fig. 8c.

Fig. 9 shows the 1D composition profile across the PAGBs in Fig. 8 along the black arrow with a bin size of 0.5 nm. The peak concentrations of carbon and boron at the PAGB of the uncracked steel are ~ 6.0 at.% C and ~ 1.0 at.% B, respectively. In contrast, the PAGB near surface region of the cracked steel was found to have the peak C concentration of ~ 5.0 at.%, while the peak B concentration as low as ~ 0.6 at.%. The carbon content on the PAGB in the center region of the cracked steel is as high as 23.0 at.%, as shown in Fig. 9c, suggesting the formation of Fe_3C , consistent with TEM observation. It is worth mentioning that the width of the Fe_3C plate on the PAGB in Fig. 8c is quite narrow, comparable to the width of the solute segregation on the PAGBs in Fig. 8a and b. The boron excess at the PAGB of the surface region of the cracked steel was 0.10 n/nm^2 , much lower than 2.22 n/nm^2 in the uncracked sample, as listed in Table 2. With formation of the boride precipitate at PAGBs, the PAGB exhibited no significant segregation of boron. In the center region of the cracked steel, only Fe_3C was found on the PAGBs.

4. Discussion

4.1. Understanding B segregation at PAGBs of boron steel

The segregation of B at PAGBs is crucial for obtaining ideal microstructures of quenched boron steels. Many factors including quenching temperature [26] grain boundary misorientation angles [27], cooling speed and alloying elements [27] have been found to affect the segregation of B at PAGBs. Although numerous researches have been made to understand B segregation at PAGBs, no consensus has yet been reached regarding if the B segregation at PAGBs is controlled predominantly by equilibrium or nonequilibrium segregations [26,27]. It is likely that both mechanisms work together to determine the real segregation, although one mechanism can be more predominant than the other depending on a specific quenching condition. Nonequilibrium segregation become predominant only if vacancies in steel are well above the equilibrium concentration, such as quenching from high temperatures [26]. Since the quenching temperature of our boron steel was 880°C ,

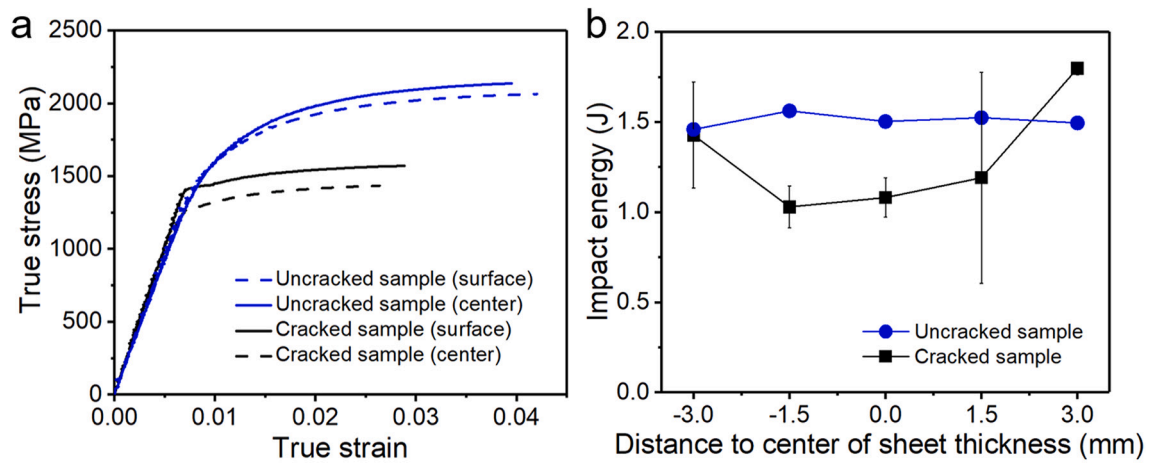


Fig. 4. Tensile test results (a) and impact test results (b) of uncracked and cracked samples at different positions across the sheet thickness.

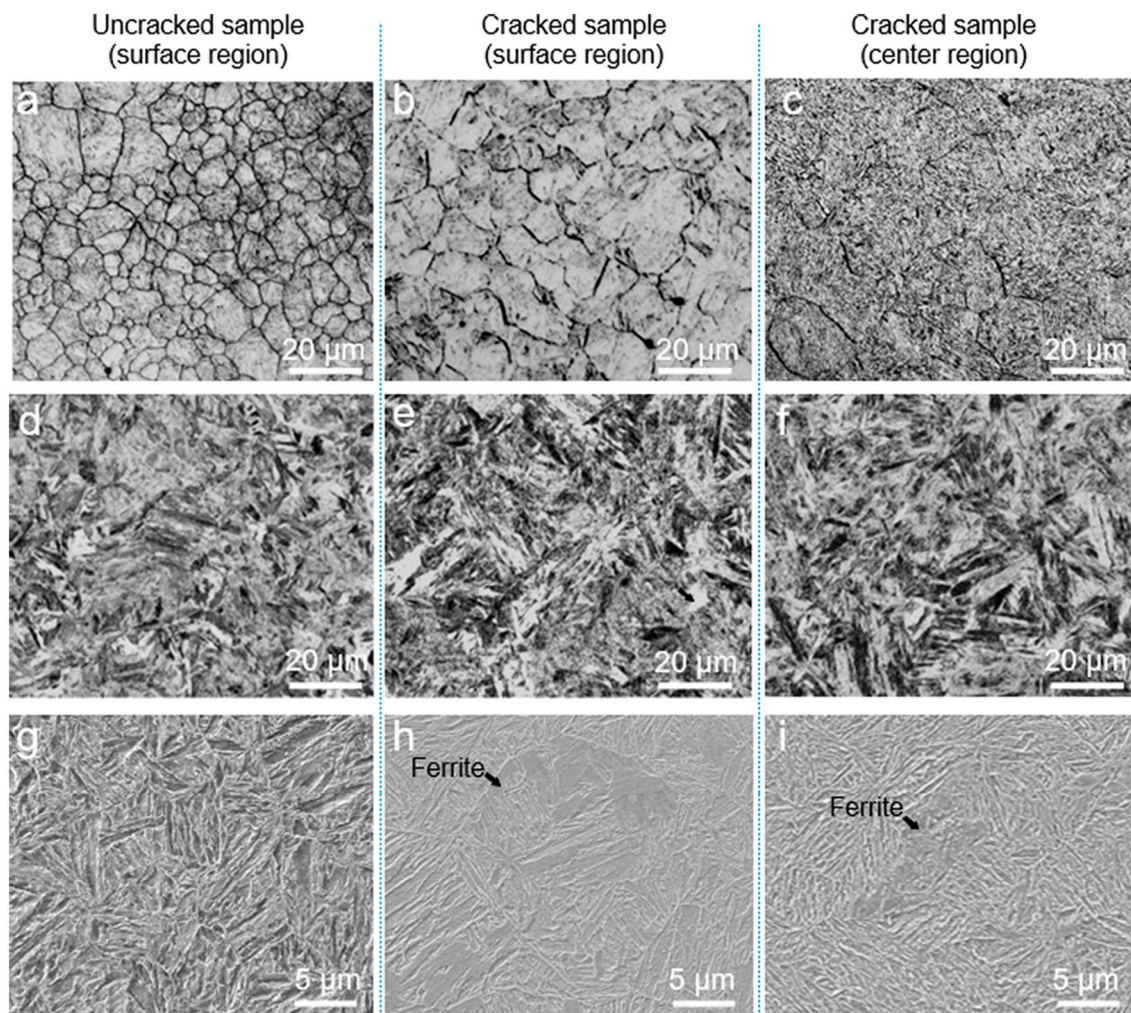


Fig. 5. OM images of austenite grain structure (a)–(c), OM images of martensite structure (d)–(f), and SEM images of an uncracked sample in surface region as well as cracked samples in surface region and center region, respectively (g)–(i).

below 950 °C reported by [27], equilibrium segregation likely became predominant in controlling the B segregation at PAGBs. Under the equilibrium segregation, B segregation at PAGBs increases at slower cooling rate if boride precipitation is avoided [27]. The observation of B excess at PAGBs in the cracked steel lower than that in uncracked steels,

as listed in Table 2, and the formation boride precipitates observed in Fig. 7, indicate that the cracked steel was cooled below its critical cooling rate.

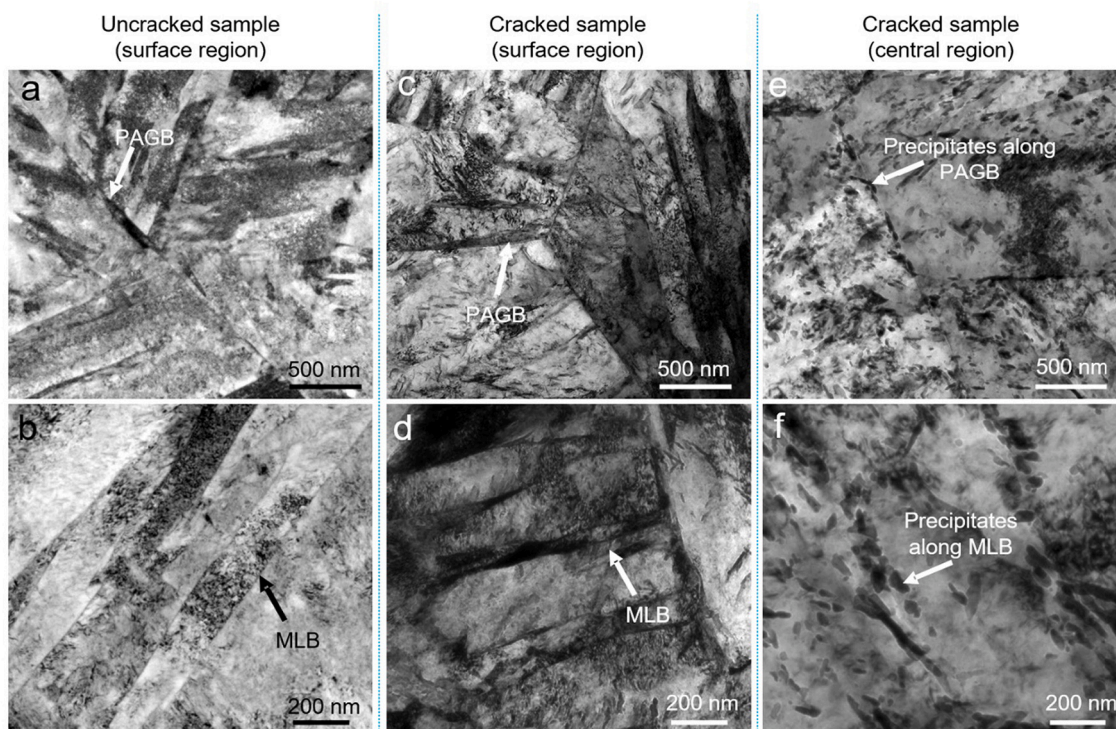


Fig. 6. Bright field TEM images of the uncracked samples from the surface region (a) and (b), as well as the cracked samples from surface regions (c) and (d), and from center regions (e) and (f).

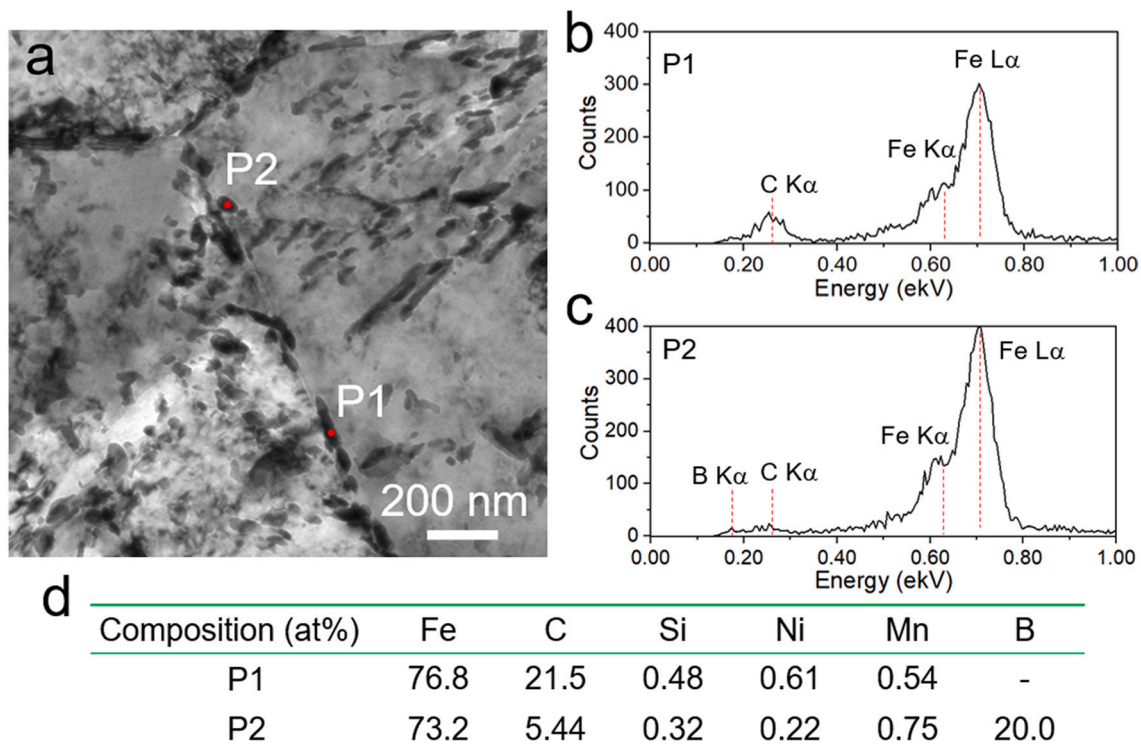


Fig. 7. BF TEM image of a sample from the center region of the cracked sheet with precipitates (a), EDS point analysis profiles (b) and (c), and measured compositions of two particles marked in the TEM image (d).

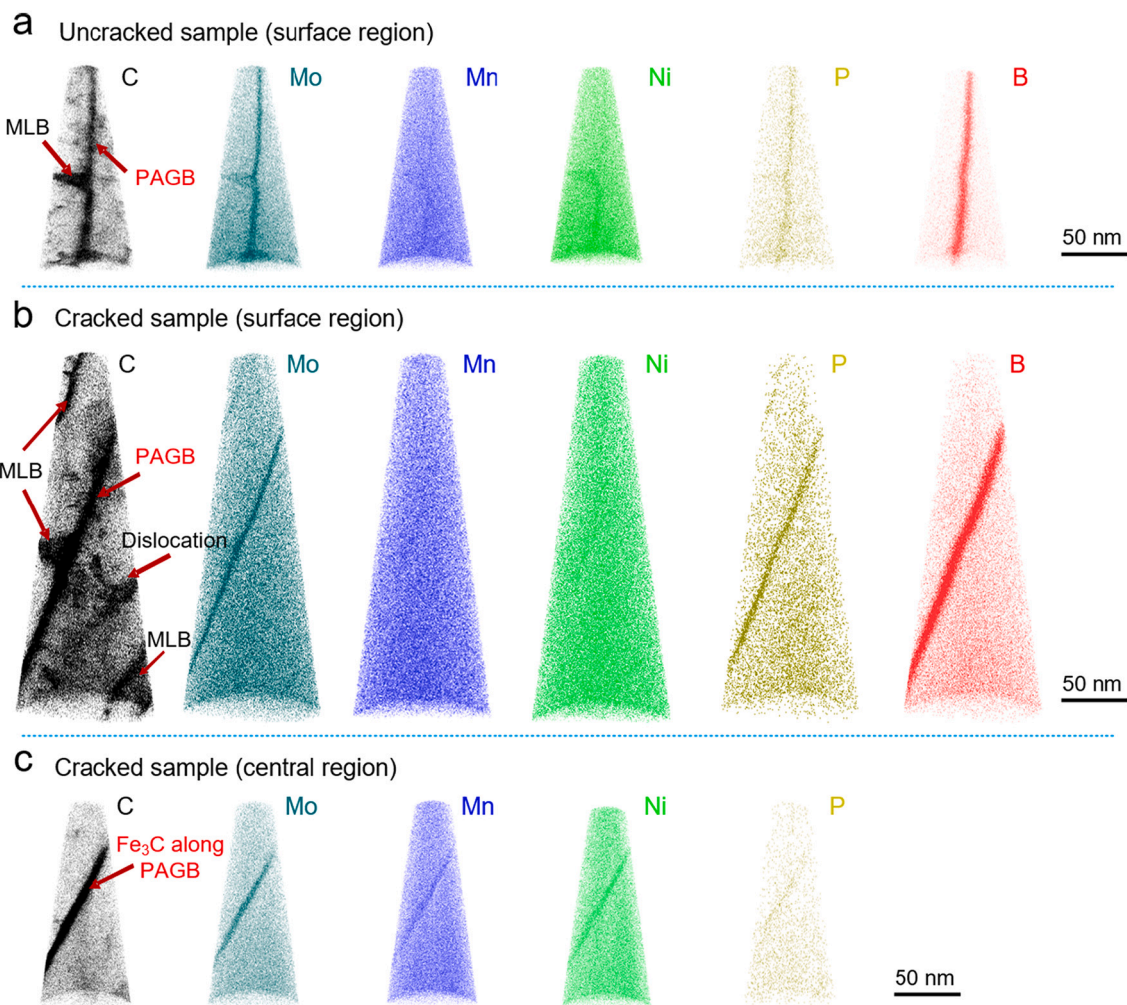


Fig. 8. APT results of atom maps of a sample from surface region of the uncracked sheet (a), as well as samples from the surface region (b), and the center regions (c) of the cracked sheet.

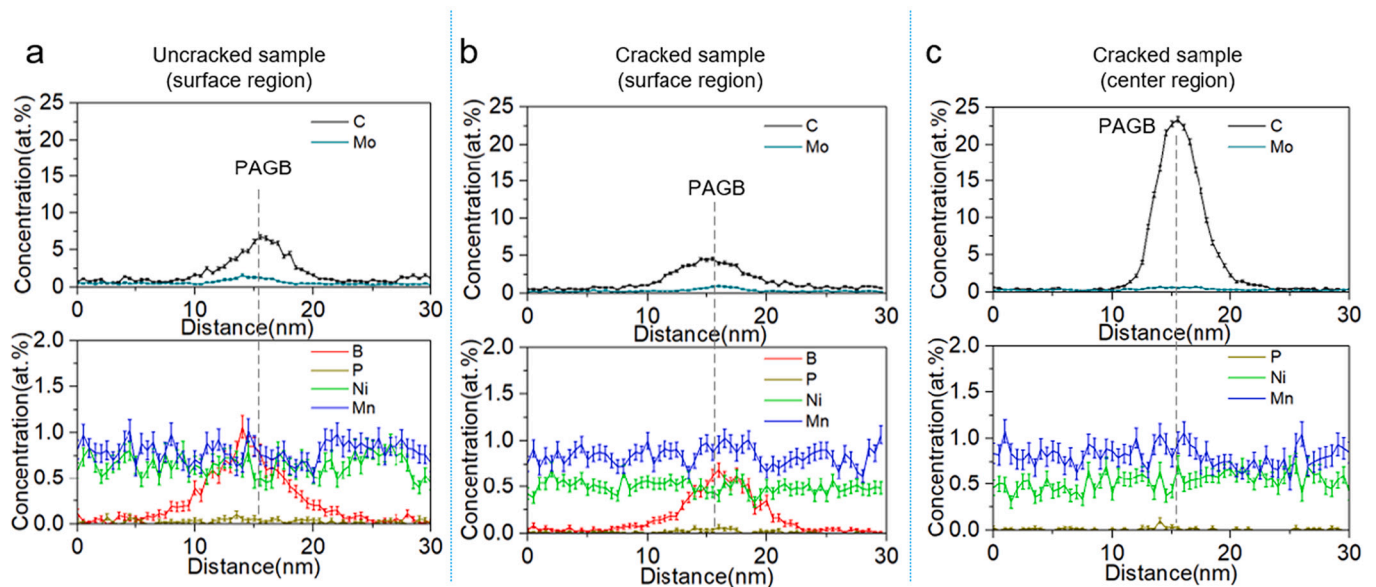


Fig. 9. 1D concentration profiles across the PAGBs in Fig. 8 of (a) surface region of the uncracked sample as well as (b) surface and (c) center regions of the cracked samples.

Table 2

Solute excess of the PAGBs of uncracked and cracked samples in Fig. 7 (atom/nm²).

| | C | B | Mo | P |
|--------------------------|---|------|------|------|
| Uncracked sample | 15.76 | 2.22 | 1.68 | 0.09 |
| Cracked sample (surface) | 21.96 | 0.10 | 0.55 | 0.08 |
| Cracked sample (center) | Fe ₃ C precipitates at PAGBs | | | |

4.2. Correlation between boron distribution at PAGBs and quench cracking

Detailed SEM examination indicates that PAGBs are the main microstructural feature directly correlated with quench-cracking of the boron steel (Fig. 3). The PAGBs of the quench-cracked steel decorated with Fe₃C and Fe₃(C, B) precipitates. In contrast, the PAGBs of the uncracked steel are segregated with boron atoms (Fig. 8). The formation of these boron-containing precipitates consumed most of the boron atoms segregated at the PAGBs, and hence the beneficial effect of boron segregation at the PAGBs on the hardenability of the steel diminished. Without sufficient B segregation at PAGBs of the cracked sample (Fig. 8), the ferrite is able to form along PAGBs as observed in Fig. 5, with a reduced fraction of martensite in the quenched structure. It has been reported that the increased ferrite fraction in ferrite and martensite duplex steel deteriorates the tensile strength and toughness due to the strength difference between ferrite and martensite [28,29]. The formation of the soft ferrite phase is well correlated with the deterioration of tensile strength of the cracked sample, as observed in Fig. 4a. Moreover, the partitioning of carbon atoms between the newly formed ferrite and the remained austenite due to the low solubility of carbon in ferrite increase the carbon content in austenite with depressed martensite transformation temperature. Formation of brittle Fe₃C particles densely distributed along the PAGBs with ferrite, as observed in the center region of the cracked steel (Fig. 7a), is easy for crack initiation under plastic deformation and responsible for the significant decrease in ductility of the steel. More Fe₃C particles formed in the center region than those in the surface region of the cracked steel are consistent with the worse impact energy of the center region.

The steel without full martensite suffered with quenching cracking along PAGBs when the internal stress from the thermal strain and volume changes of the phase transformation from austenite into martensite [30,31] was greater than the ultimate strength of the steel. The deteriorated mechanical properties of the cracked steel with the formation of ferrite and Fe₃C on PAGBs made cracks easily to initiate and propagate along the PAGBs during quenching.

4.3. Correlation between processing factors and distribution of boron

As shown in Fig. 4a–c, the austenite grain sizes in the cracked sample are much larger than that in the uncracked sample. According to [32,33], the hardenability increases with increasing austenite grain size, because the decrease of grain boundary area would reduce the sites for the nucleation of ferrite and pearlite. On the other hand, the reduction of grain boundary area will increase the solute segregation level per unit area, which facilitates the precipitation on the PAGBs. In the uncracked sample with the smallest austenite grain size ~6.4 μm, no boron-containing precipitates but only segregation of boron atoms can be found at PAGBs. However, in the surface region of the cracked steel with a large austenite grain size ~12.6 μm, the boron-containing precipitates formed and the boron segregation at PAGBs significantly decreased, as shown in Table 2. The center position of the cracked sample has the largest austenite grain size ~16.5 μm, with PAGBs without any boron segregation. The coarse austenite grains in the cracked steel could form due to longer holding in austenite region. Clearly, the enhanced hardenability of the cracked steel with the coarse austenite grains was insufficient to ease the precipitation on the PAGBs, and the lost B

segregation was probably due to insufficient cooling rate during the quenching.

The cooling rate during quenching also influences the boron distribution at PAGBs. It has been reported in [34] that no precipitates can be observed on grain boundaries when steels are water-quenched (cooling rate of 90,000 °C/min) after hot-rolling at 1300 °C. However, boron-containing precipitates such as M₂₃(C, B)₆ and BN can form on austenite grain boundaries at relatively lower cooling rates. As shown in Fig. 6, compared to the center position, the surface position of the cracked steel has a less amount of precipitates formed, which suggests that the inadequate cooling rate could be the main reason for the formation of boron-containing precipitates and thus the quench cracking.

5. Conclusions

Multi-scale microstructural characterizations and mechanical property tests were implemented on boron steels sheets (6 mm in thickness) with/without quenching cracking to reveal microstructural origins for quench cracking of the steel, with conclusions as follow:

1. Quench cracking of the steel sheet is brittle intergranular fracture in nature, along prior austenite grain boundaries (PAGBs).
2. Microscopically, quenching cracking is highly related with the distribution of B in the microstructure of the steel. The segregation of boron on the PAGBs is essential for easing quench cracking.
3. Formation of boron-containing precipitates Fe₃(C,B) precipitates consumed most B atoms segregated at PAGBs, and facilitated the formation of ferrite and massive acicular-shaped Fe₃C in the steel during quenching. The quenched steel with the PAGBs decorated with precipitates suffered with deterioration in mechanical properties and quench cracking as a result.
4. The insufficient cooling rate probably is the main reason for the formation of boron-containing precipitates on PAGBs and thus the quench cracking.

Data availability statement

The raw/processed data required to reproduce these findings cannot be shared at this time as the data also forms part of an ongoing study.

Declaration of Competing Interest

This letter is to submit our manuscript entitled “Microstructural origins for quench cracking of a boron steel: Boron distribution”, in consideration for publication in Materials Characterization. This article reports our original research. No part of it has submitted or considered to be submitted to other journal.

The authors declare that we have no known competing financial interests or personal relationships that could have appeared to influence the work reported in this paper.

Acknowledgment

Authors would like to thank Nanjing iron and steel Co., Ltd. for sponsoring this research project. The authors would like to acknowledge facility use and scientific and technical assistance from the Materials Characterization Facility in Nanjing University of Science and Technology.

References

- [1] M. Sharma, I. Ortlepp, W. Bleck, Boron in heat-treatable steels: a review, *Steel Res. Inter.* 90 (2019) 1900133.
- [2] D.T. Llewellyn, W.T. Cook, Metallurgy of boron-treated low-alloy steels, *Metals Technol.* 1 (1974) 517–529.

- [3] A. Terzic, M. Calcagnotto, S. Guk, T. Schulz, et al., Influence of boron on transformation behavior during continuous cooling of low alloyed steels, *Mater. Sci. Eng. A* 584 (2013) 32–40.
- [4] S. Koley, A. Karani, S. Chatterjee, M. Shome, Influence of boron on austenite to ferrite transformation behavior of low carbon steel under continuous cooling, *J. Mater. Eng. Perform.* 27 (2018) 3449–3459.
- [5] A. Brown, J.D. Garnish, R.W.K. Honeycombe, The distribution of boron in pure iron, *Metal Sci.* 8 (1974) 317–324.
- [6] T.M. Williams, A.M. Stoneham, D.R. Harries, The segregation of boron to grain boundaries in solution-treated type 316 austenitic stainless steel, *Metal Sci.* 10 (1976) 14–19.
- [7] X.M. Wang, X.L. He, Effect of boron addition on structure and properties of low carbon bainitic steels, *ISIJ. Inter.* 42 (2007) 38–46.
- [8] N.D. Luozzo, M. Schulz, M. Fontana, Imaging of boron distribution in steel with neutron radiography and tomography, *J. Mater. Sci.* 55 (2020) 7927–7937.
- [9] G. Shigesato, T. Fujishiro, T. Hara, Grain boundary segregation behavior of boron in low-alloy steel, *Metall. Mater. Trans. A* 45 (2014) 1876–1882.
- [10] D.J. Mun, E.J. Shin, K.C. Cho, J.S. Lee, et al., Cooling rate dependence of boron distribution in low carbon steel, *Metall. Mater. Trans. A* 43 (2011) 1639–1648.
- [11] B. Białobrzęska, Effect of alloying additives and microadditives on hardenability increase caused by action of boron, *Metals* 11 (2021) 589.
- [12] L. Lanier, G. Metauer, M.J.M.A. Moukassi, Microprecipitation in boron-containing high-carbon steels, *Microchim. Acta* 114 (1994) 353–361.
- [13] J.P.G. Antunes, C.A. Nunes, Characterization of impact toughness properties of DIN39MnCrB6-2 steel grade, *Mater. Res.* 21 (2017) 1–5.
- [14] T. Manabe, S. Yamasaki, S. Nishida, T. Sugawara, et al., Effect of boron addition for on time temperature transformation behavior in Si added high carbon steels, *ISIJ. Inter.* 60 (2020) 1796–1802.
- [15] G.F. Melloy, P.R. Summon, P.P. Podgursky, Optimizing the boron effect, *Metall. Trans. A* 4 (1973) 2279–2289.
- [16] K. Yamanaka, Y. Ohmori, Effect of boron on transformation of low-carbon low-alloy steels, *Tetsu to Hagane* 62 (1976) 895–904.
- [17] H. Asahi, Effects of Mo addition and austenitizing temperature on hardenability of low alloy B-added steels, *ISIJ. Inter.* 42 (2002) 1150–1155.
- [18] J. Sun, H. Zhu, W. Wang, Y. Duan, Effect of boron segregation on the surface crack of low carbon boron-bearing steel, *Res. Phys.* 13 (2019), 102153.
- [19] K. Yamamoto, H.G. Suzuki, Y. Oono, T. Inoue, Formation mechanism and prevention method of facial cracks of continuously cast steel slabs containing boron, *Tetsu to Hagane* 73 (1987) 115–122.
- [20] K.C. Cho, D.J. Mun, J.Y. Kim, J.K. Park, et al., Effect of boron precipitation behavior on the hot ductility of boron containing steel, *Metall. Mater. Trans. A* 41 (2010) 1421–1428.
- [21] K.C. Cho, D.J. Mun, M.H. Kang, J.S. Lee, et al., Effect of thermal cycle and nitrogen content on the hot ductility of boron-bearing steel, *ISIJ. Inter.* 50 (2010) 839–846.
- [22] K. Taguchi, S. Takaya, M. Numata, T. Kato, Effect of deoxidizing element on the hot ductility of boron-containing steel, *ISIJ. Inter.* 60 (2020) 2829–2837.
- [23] A. Gramlich, C.V.D. Linde, M. Ackermann, W. Bleck, Effect of molybdenum, aluminium and boron on the phase transformation in 4 wt.-% manganese steels, *Res. Mater.* 8 (2020), 100147.
- [24] S.N. Ghali, H.S. El-Faramawy, M.M. Eissa, Influence of boron additions on mechanical properties of carbon steel, *J. Miner. Mater. Charact. Eng.* 11 (2012) 995–999.
- [25] I.B. Timokhina, M.K. Miller, H. Beladi, P.D. Hodgson, The influence of fine ferrite formation on the γ/α interface, fine bainite and retained austenite in a thermomechanically-processed transformation induced plasticity steel, *J. Mater. Res.* 31 (2016) 806–818.
- [26] G. Miyamoto, A. Goto, N. Takayama, T. Furuhashi, Three-dimensional atom probe analysis of boron segregation at austenite grain boundary in a low carbon steel-effects of boundary misorientation and quenching temperature, *Scr. Mater.* 154 (2018) 168–171.
- [27] J. Takahashi, K. Ishikawa, K. Kawakami, M. Fujioka, et al., Atomic-scale study on segregation behavior at austenite grain boundaries in boron-and molybdenum-added steels, *Acta Mater.* 133 (2017) 41–54.
- [28] S. Wang, H. Yu, T. Zhou, L. Wang, Synergetic effects of ferrite content and tempering temperature on mechanical properties of a 960 MPa grade HSLA steel, *Mater.* 11 (2018) 2049.
- [29] H. Li, S. Gao, Y. Tian, D. Terada, et al., Influence of tempering on mechanical properties of ferrite and martensite dual phase steel, *Mater. Today., Proc.* 2 (2015) S667–S671.
- [30] E. Hornbogen, Martensitic transformation at a propagating crack, *Acta Metall.* 26 (1978) 147–152.
- [31] J.M. Moyer, G.S. Ansell, The volume expansion accompanying the martensite transformation in iron-carbon alloys, *Metall. Trans. A* 6 (1975) 1785.
- [32] X. Li, X. Ma, S.V. Subramanian, C. Shang, et al., Influence of prior austenite grain size on martensite-austenite constituent and toughness in the heat affected zone of 700 MPa high strength linepipe steel, *Mater. Sci. Eng. A* 616 (2014) 141–147.
- [33] X.C. Li, D.X. Xia, X.L. Wang, X.M. Wang, et al., Effect of austenite grain size and accelerated cooling start temperature on the transformation behaviors of multi-phase steel, *Sci. China Technol. Sci.* 56 (2012) 66–70.
- [34] S. Watanabe, H. Ohtani, Precipitation behavior of boron in high strength steel, *Trans. ISIJ.* 23 (1983) 38–42.